Dynamic EIS of Fuel Cells under Transient Operating Conditions for Fault Detection

Jules MILLET*[1], Daniel DEPERNET[1], Ali SARI[2], Frédéric GUSTIN[1], and Hugo HELBLING[2]

[1]Université Marie et Louis Pasteur, UTBM, CNRS, Institut FEMTO-ST, F-90000 Belfort, France
[2]Université Claude Bernard Lyon 1, Ampère, UMR5005, INSA Lyon, Ecole Centrale de Lyon, CNRS, Villeurbanne, F-69100, France

Abstract

This study investigates the impedance behavior of fuel cells under varying current conditions, with the aim of developing and evaluating a dynamic EIS-based fault detection methodology. Stationary Electrochemical Impedance Spectroscopy measurements were first carried out under controlled conditions to characterize the dependence of impedance on current. Based on Equivalent Circuit Models and polynomial approximations, an experimental current-dependent impedance model was established to assess the validity of impedance measurements under dynamic operating conditions. To compute impedance in this non-stationary regime, a dedicated signal processing algorithm was developed. The algorithm compensates for drift effects induced by non-stationarity and enables impedance estimation over short time windows, without requiring the control system to be held at a stationary operating point. Finally, representative driving cycles were applied to identify impedance spectra under dynamic conditions using the proposed model. The results are promising and confirm the relevance of the developed approach.

Keywords: Dynamic EIS, Fuel cell diagnostics, Current-dependent impedance model, Signal processing, Fault detection

*Corresponding author. E-mail: jules.millet@utbm.fr

1 Introduction

As part of the energy transition, reducing environmental impacts in the transport sector represents a major challenge [1]. The electrification of transport, driven by battery-powered vehicles, is a key lever to address this issue. At the same time, hydrogen vehicles, which are currently experiencing significant growth, complement the electric mobility landscape.

Electric vehicles do not produce CO_2 emissions during use, but they have non-negligible environmental impacts associated with raw material extraction, component manufacturing, and end-of-life management of the systems. However, the deployment of hydrogen vehicles raises several challenges, particularly those related to fuel cells, which are the core component of the propulsion system [2].

Optimizing the use of fuel cells is therefore a key issue to extend their lifetime, provided that their state of health can be assessed and the defects contributing to their aging can be detected [3, 4]. In this context, ensuring reliability and real-time diagnostics becomes essential. Among the available methods, EIS stands out for its ability to identify internal processes over a wide frequency range and is widely recognized for aging characterization and fault detection [5, 6].

However, implementing EIS in an embedded environment remains complex [7]. The generation of an excitation signal and the maintenance of the fuel cell in a steady state require specific technical means. Several studies have proposed locking the control at an operating point to inject the signal via the power converter [7, 8], thus complying with the EIS application conditions. Nevertheless, this approach reduces vehicle availability, since the fuel cell can no longer follow the power demand during the impedance measurement. Moreover, the excitation signal generation and the associated voltage and current measurements must be coordinated with the power converter control strategy. This requirement generally increases implementation complexity and may require modifications to the system control architecture.

To overcome these limitations, dynamic EIS appears as a promising approach since it does not require control blocking. Several approaches have been investigated in the literature to facilitate onboard impedance measurements. Converter-based EIS methods provide accurate impedance measurements but generally require synchronization and operating-point locking [8, 7]. Multi-sine approaches reduce measurement duration and improve compatibility with dynamic operation [9, 10]. Passive EIS methods eliminate the need for external excitation but are strongly dependent on the spectral content naturally present in the system [11, 12]. Recent studies have also investigated data-driven approaches for predicting PEMFC impedance under varying operating conditions. These approaches have demonstrated the ability of advanced learning models to capture the nonlinear relationship between operating conditions and impedance spectra. Such works highlight the growing interest in impedance-based modeling and monitoring of fuel cells [13]. These limitations motivate the development of a dynamic EIS approach combining active excitation with signal processing techniques inspired by passive EIS.

Already explored in the field of batteries [9, 10], this approach requires knowledge of the impedance behavior under dynamic conditions. In parallel, passive EIS methods have introduced signal processing techniques capable of estimating impedance without synchronization [11, 14]. These techniques provide valuable insights for onboard implementation under dynamic operating conditions.

Unlike existing converter-based EIS methods based on operating-point locking, the proposed approach aims to perform electrochemical impedance spectroscopy under transient operating conditions. The proposed methodology is based on a dedicated signal-processing algorithm inspired by passive EIS techniques, capable of compensating for drift and extracting impedance without interrupting the normal operation of the fuel cell. To interpret the estimated impedance and provide a healthy reference for fault detection, a current-dependent impedance model is identified from experimental EIS measurements. The proposed methodology is finally evaluated for fault detection under representative driving conditions.

The main contributions of this work are summarized as follows:

- A dynamic EIS methodology for impedance estimation under transient operating conditions;
- A drift-compensated signal-processing algorithm inspired by passive EIS techniques;
- A current-dependent impedance model providing the healthy reference required for dynamic impedance interpretation and fault detection;
- Validation of the proposed methodology within a fuel cell simulation framework;
- Application of the methodology to fault detection under the Lyon-Milan driving cycle.

To address these challenges, the first section presents the phenomena responsible for the non-stationary behavior of the system and their impact on impedance measurements. Existing methods for estimating impedance under dynamic operating conditions are then reviewed, before introducing the proposed dynamic EIS approach and its associated signal processing algorithm.

The proposed methodology combines experimental impedance characterization with dynamic impedance estimation under transient operating conditions. Experimental EIS measurements acquired on a healthy fuel cell stack at different steady-state current operating points are first used to identify a current-dependent impedance model, providing the healthy reference required for fault detection. This model is then integrated into a dynamic fuel cell simulation framework to reproduce realistic operating conditions and various fault scenarios. Within this validation framework, the proposed signal-processing algorithm is applied to estimate impedance under dynamic operating conditions. Finally, the estimated impedance spectra are compared with the healthy reference model to evaluate the feasibility of fault detection on representative driving cycles, including the Lyon-Milan route.

2 Factors Affecting Non-Stationarity and Their Effects on Electrochemical Impedance

Electrochemical impedance spectroscopy is widely used as a tool to study electrochemical phenomena [15]. This technique involves applying an excitation signal at a given frequency around an operating point. By analyzing both the voltage and current responses, the impedance at the injected frequency can be calculated. Repeating this process over a defined frequency range produces the impedance spectrum.

EIS is particularly relevant when the system is under steady-state conditions, meaning that the factors influencing impedance (current, temperature, stoichiometry, relative humidity, state of health, etc.) remain stable. These steady-state conditions are essential to ensure the validity and reproducibility of the measurements [16].

However, this requirement becomes a limitation when the system operates under dynamic conditions. Indeed, variations in the operating conditions continuously modify the fuel cell impedance during the measurement. As a result, the assumption of a stationary system is no longer strictly valid, which makes the interpretation of impedance spectra significantly more challenging [17, 18]. Therefore, it is first useful to identify how impedance evolves under different steady-state conditions as a function of key operating parameters such as current, temperature, stoichiometry, and relative humidity. This helps build a better understanding of the responses observed later under dynamic conditions.

To further analyze the internal phenomena within the cell, ECMs are used to associate specific electrochemical processes with electrical components [19, 20]. Each parameter, or combination of parameters, can thus be linked to a particular electrochemical process (Figure 1). Consequently, depending on the different operating conditions, it becomes possible to track the evolution of these parameters and interpret the underlying internal mechanisms.

Well studied in the literature [17, 21], the impedance spectrum of a fuel cell can generally be divided into four distinct parts (Figure 1):

- Region 1: At high frequencies, the ohmic resistance reflects the resistance of the membrane and the electrical contacts;
- Region 2: Charge transfer process and double-layer capacitance: reflects the kinetics of electrochemical reactions at the anode;
- Region 3: Charge transfer process and double-layer capacitance: reflects the kinetics of electrochemical reactions at the cathode;
- Region 4: Mass transport limitations, mainly associated with oxygen diffusion phenomena in the cathode.

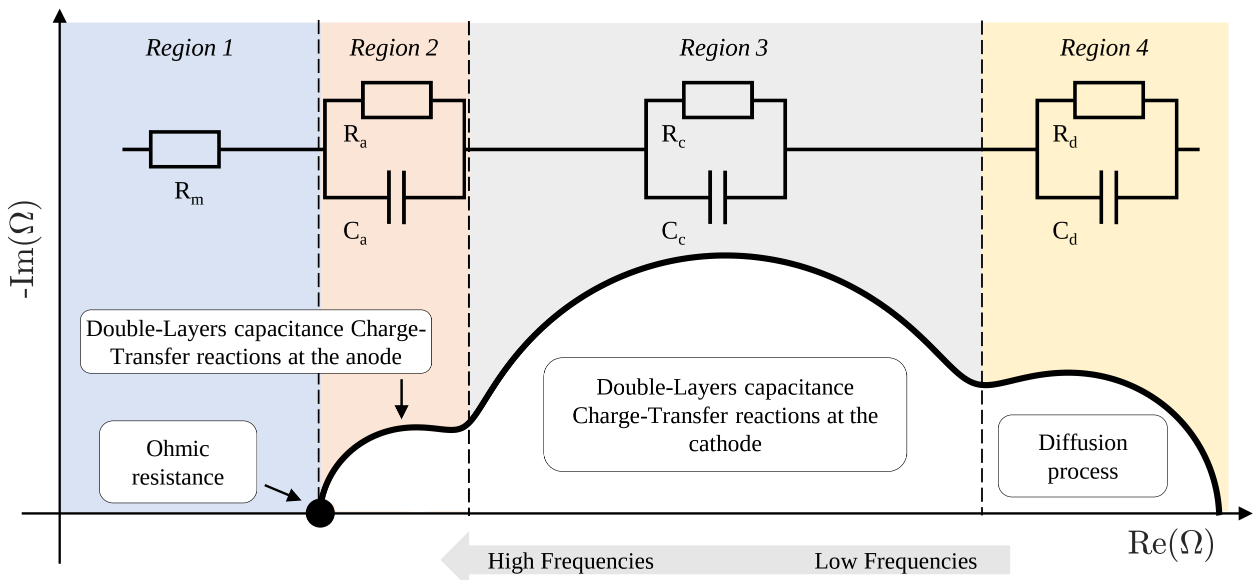

Figure 1: Nyquist diagram from EIS with the corresponding Equivalent Circuit Model.

Several studies on fuel cells highlight variations in impedance depending on different operating conditions (current, temperature, stoichiometry, relative humidity). These studies focus on fault detection in these systems and present tests carried out under these various conditions, helping to identify which section is affected in each case [5].

Other papers complement and strengthen this analysis [22, 23, 24, 25]:

- Current: slight decrease in charge transfer resistance on the cathode side, and a strong impact on the diffusion process;
- Temperature: affects both the cathodic charge transfer resistance and the diffusion process. Higher temperatures generally improve reaction kinetics and reduce the charge transfer resistance, while also influencing mass transport phenomena;

- Stoichiometry: when stoichiometry decreases, the diffusion-related lobe diminishes, and conversely, it increases when stoichiometry rises;

- Relative humidity: mainly affects the diffusion region.

These observations highlight the variation of impedance for each parameter studied. It is difficult to determine which factor is the most influential since, as shown in various studies, each parameter affects the system differently depending on whether the current is high or low.

This analysis is particularly valuable for fault detection within the system, as such faults can be identified through impedance analysis, especially in the diffusive region.

Having characterized impedance behavior for different parameters under steady-state conditions, the next step is to determine suitable analysis methods capable of extracting impedance under dynamic operating conditions. These methods can then be used together with current-dependent impedance models to investigate impedance estimation under transient operating conditions.

3 Embedded Impedance Measurement

With the goal of determining impedance under dynamic conditions, a study was conducted on the key components required to perform EIS under steady-state operation, namely: an excitation source and a signal processing algorithm. These two elements enable the implementation of EIS. However, when applied in an embedded system, they must be adapted to ensure proper operation under such conditions.

3.1 Excitation through the Power Converter

This subsection reviews existing approaches based on power converter excitation and highlights their limitations regarding synchronization and operating constraints.

The current stimulus is at the core of EIS. Without it, no EIS measurement can take place. One approach already explored in the literature involves using the DC/DC converter located between the fuel cell and the DC bus to generate the excitation signal [26, 27]. This method relies on Pulse-Width Modulation (PWM) to inject the signal [8].

In this configuration, the converter control is held fixed to operate in steady-state conditions, which allows the injection of the current stimulus. However, this setup requires strict synchronization between the power converter control, which generates the excitation signal, and the voltage and current acquisition system used for impedance estimation. In practical applications, this often implies a tight coordination between the power electronics, the energy management system, and the measurement unit. Such synchronization is required to accurately identify the frequencies and phases of the injected harmonics.

For the Discrete Fourier Transform to correctly identify these components, the analysis window must be aligned with the excitation signal and contain an exact number of periods. Any timing mismatch between signal generation and signal acquisition may introduce phase and amplitude errors, resulting in spectral leakage and biased impedance estimates [8].

This constraint represents a major limitation, and it is precisely one of the key areas addressed in this study. The proposed method eliminates the need for synchronization between excitation signal generation and impedance estimation, as well as control blocking conditions, while maintaining the ability to effectively inject the current stimulus.

3.2 Exploitation of Harmonics

EIS is a characterization method for electrochemical sources, whether fuel cells or batteries. In both cases, the underlying principles are similar: what applies to one can, to a large extent, be transferred to the other. This means that methods developed for batteries can be adapted for fuel cells, and conversely.

However, it is important to remember that impedance behaves differently depending on the operating conditions specific to each technology. That is exactly why the previous section focused on analyzing the specific impedance behavior of the fuel cell. The method identified in the following part of the study was therefore developed based on dynamic EIS studies reported for both batteries and fuel cells. A literature review was carried out on dynamic EIS and the associated impedance calculation methods.

First, this study proposes characterizing the fuel cell using polarization curves and EIS measurements [4]. It highlights how the spectra evolve over time as aging occurs. This represents an interesting first approach, but the EIS measurements are performed only at fixed operating points using conventional signal processing algorithms.

In another study [25], the influence of excitation signal amplitude on impedance estimation was investigated. It was shown that excessively large amplitudes may induce operating-point variations during the measurement, leading to distortions in the estimated frequency response. Although the study proposes guidelines for selecting an appropriate excitation amplitude, it does not provide a signal processing method to compensate for these effects.

As mentioned earlier, it is therefore useful to turn to battery research, which has been ongoing for many years, to explore the concept of dynamic EIS and the related algorithms.

Another contribution in the literature reports real-time EIS measurements performed on batteries subjected to a dynamic current profile [9]. Their method accounts for dynamic effects by speeding up the EIS measurement (multi-sine approach), which helps reduce drift time. This work highlights the importance of developing algorithms capable of correcting these drifts during analyses under dynamic conditions. Along the same lines, other studies have also emphasized the benefits of such compensation [16].

Furthermore, as part of a non-intrusive diagnostic approach, several studies on batteries have focused on developing passive impedance estimation algorithms, allowing system characterization without disrupting its operation.

In this context [11, 12, 28], extended this approach by estimating the impedance of a lithium-ion battery using natural harmonics present in driving cycles, based on power spectral density analysis. Their method, which relies on signal segmentation, mainly provides access to impedance at high frequencies (100 Hz to 1 kHz). A major advantage of this approach is that it requires neither prior knowledge of the frequencies of interest nor synchronization with any externally generated excitation signal. This strategy, known as passive EIS, is based on exploiting the naturally occurring frequency content in the system without any external excitation.

These studies highlight a crucial need: to develop a signal processing algorithm capable of quickly estimating impedance from the harmonics generated by the converter, under dynamic conditions, while also compensating for drift. The existing approaches, originally designed for batteries, provide a solid foundation that can be adapted to fuel cells.

Although passive EIS approaches rely on naturally occurring harmonics, the signal processing techniques developed in this field are particularly relevant to the present work. Indeed, they address challenges similar to those considered here, such as impedance estimation under dynamic operating conditions without requiring synchronization between excitation generation and impedance estimation. The proposed method therefore builds upon these signal processing concepts but does not rely on naturally occurring harmonics. Instead, it exploits harmonics generated by the power converter.

3.3 Detailed Algorithm

To meet the constraints of embedded systems, a rigorous methodology was developed to ensure reliable impedance estimation under dynamic operating conditions. The proposed approach builds upon signal processing methods previously developed for passive EIS applications [11, 14], while introducing several key contributions, including automatic identification of the excitation frequencies without prior knowledge of the injected frequencies, fast EIS processing, and signal drift compensation.

The remainder of this section describes the different stages of the proposed signal processing methodology, from time-domain measurements to impedance estimation (Figure 3).

- *Step 1 : Drift Compensation*: During an impedance measurement, any variation in the system steady state can cause a gradual drift in the voltage response [16]. This drift is associated with slow phenomena such as thermal or operating condition variations and may bias impedance estimation, particularly at low frequencies. To compensate for this effect, the drift component is first estimated using a low-pass filter and then subtracted from the original signal. The cutoff frequency is selected to separate the non-stationary drift from the frequency band of interest while minimizing the impact on the impedance information to be estimated.

- *Step 2: Segmentation*: The voltage and current time-series are divided into multiple partially overlapping segments prior to spectral analysis [29]. The segment duration is selected according to the frequency band of interest in order to provide an adequate frequency resolution for the subsequent Fast Fourier Transform (FFT). Since the frequency resolution is inversely proportional to the observation window length, longer segments are required for low-frequency analysis, whereas shorter segments are sufficient for medium- and high-frequency ranges. Consequently, three different segment lengths are defined such that :

$$T_{\mathrm{LF}} > T_{\mathrm{MF}} > T_{\mathrm{HF}},$$

  where T_{LF}, T_{MF}, and T_{HF} denote the segment durations associated with the low-, medium-, and high-frequency bands, respectively.

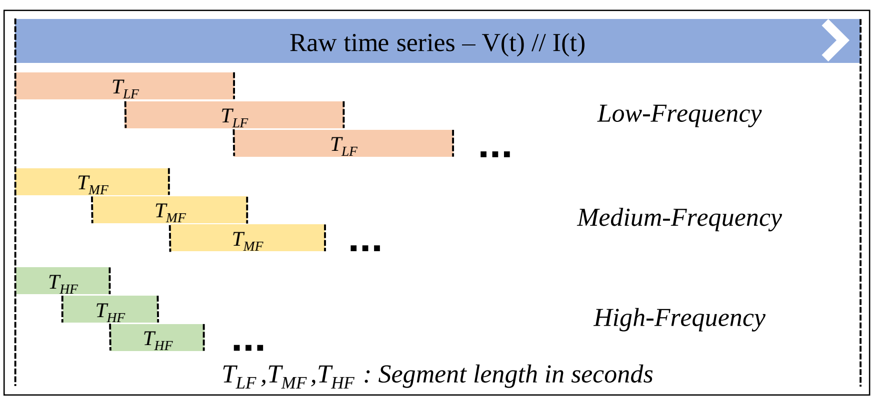

Figure 2: Segmentation of voltage and current signals into overlapping windows of different lengths for low-, medium-, and high-frequency analysis.

For each frequency range, the signals are segmented using the corresponding window length, and a predefined overlap ratio is applied between consecutive segments. This overlap increases the number of available realizations while preserving temporal continuity and improving the robustness of the spectral estimates. Each segment is then independently transformed into the frequency domain using an FFT. The overall segmentation strategy is illustrated in Figure 2.

- *Step 3 : FFT & Amplitude detection*: A windowing function is applied to each voltage and current signal segment in order to limit spectral leakage and reduce discontinuities at the segment boundaries. Since the analyzed signals are dynamic, windows such as Hamming, Hanning, or Gaussian can be used to smooth edge effects and improve spectral quality. The FFT is then applied to each windowed segment to obtain its frequency spectrum. The frequencies associated with the injected excitation signal are subsequently identified by applying a minimum amplitude threshold. This threshold is defined as a percentage of the injected AC current amplitude, ensuring that only frequency components carrying a sufficient excitation level are retained for impedance calculation while rejecting low-energy components dominated by noise. In this study, the threshold was set to 10% of the injected AC current amplitude.

- *Step 4 : Averaging*: Averaging helps smooth out random fluctuations caused by noise or signal variability. It also provides a mean impedance value for each detected frequency, calculated over a time window shorter than the time constants [17] of the stack operating parameters (temperature, stoichiometry, relative humidity, current), to improve measurement reliability. Because of overlapping segments, the same frequency can appear in several consecutive segments, averaging thus becomes essential to obtain a more precise and robust impedance estimate.

By following these steps, impedance estimation becomes possible. It is worth noting that analyzing a frequency range rather than a single harmonic allows multiple frequencies to be identified within the same segment. As a result, several excitation frequencies can be processed simultaneously, significantly reducing the time required for EIS measurements.

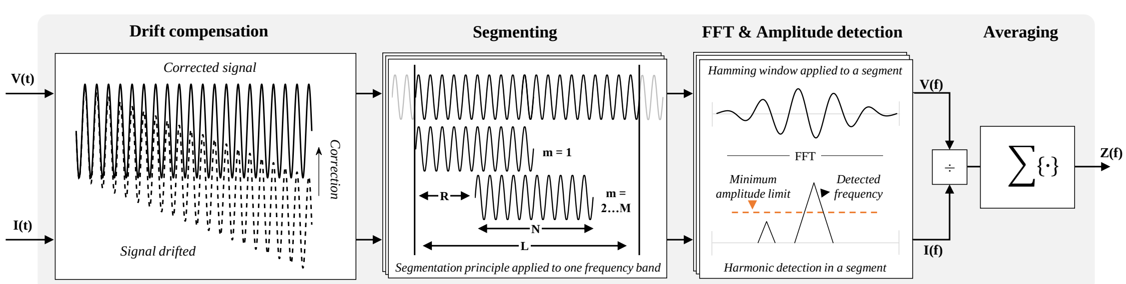

Figure 3: Optimized signal processing algorithm.

In Figure 3, N represents the number of points in the segment, R the overlap rate, L the total number of points, and M the number of segments in L.

Once the algorithm has been introduced, it can be configured. Some parameters are critical and must be defined beforehand, as they play a key role in significantly improving spectral accuracy.

3.3.1 Frequency Ranges

The frequency ranges are determined by a few key factors: the number of points per period required at the lowest and highest detectable frequencies in each band and the available computation time. To maintain reliable impedance measurements, a minimum of 8 points per period is imposed. To prevent overly long computations, the number of points per period is capped at 128. Taking these constraints into account, and using equation 1, several distinct frequency ranges can be defined.

$$F = \frac{F_s \cdot N_{prds}}{N_{pts} \cdot Dec} \tag{1}$$

Let N_{pts} denote the minimum or maximum number of points required for the detected frequency in each range, N_{prds} the number of periods of the frequency to be detected, F_s the sampling frequency, F the minimum or maximum frequency to be detected, and Dec the decimation factor.

It is nonetheless essential to first define the overall frequency range in order to capture the electrochemical phenomena of interest. Indeed, it's important to identify which phenomena can be detected based on the frequencies being analyzed. As mentioned earlier, the diffusion phenomenon is strongly influenced by temperature, current, and the state of health of the fuel cell [17]. This effect mainly appears at low frequencies, typically on the order of a few hertz. On the other hand, the ohmic resistance plays a key role in tracking impedance variations, which are generally observed around 500 hertz.

Given the characteristics of the system used, the frequency range was set from 0.1 Hz to 1000 Hz. Three sub-ranges were defined:

- A Low-Frequency (LF) range, from 0.1 Hz to 10 Hz
- A Mid-Frequency (MF) range, from 10 Hz to 100 Hz
- A High-Frequency (HF) range, from 100 Hz to 1000 Hz

Although the low-frequency range is defined between 0.1 and 10 Hz, the lowest injected frequency considered in this study is 0.6 Hz. The cut-off frequency of the drift compensation filter therefore remains below the frequency components used for impedance estimation.

By measuring voltage and current and applying the appropriate decimation factors, it becomes possible to obtain the required number of points for each segment, and therefore to calculate the impedance with sufficient resolution.

3.3.2 Cutoff Frequency: Drift Filter

Drift compensation is achieved by applying a low-pass filter, whose role is to separate the slow components related to non-stationary drift from those associated with the EIS excitation. To do this, it is necessary to identify an appropriate cutoff frequency. This frequency effectively distinguishes slow dynamics from those of interest in the measurements. A Butterworth filter is used for this operation because of its smooth frequency response. For each of the three analyzed frequency ranges, a specific cutoff frequency is determined based on the minimum frequency of the corresponding range (Table 1). In the low-frequency range, the cutoff frequency is set to 0.1 Hz in order to observe the maximum frequency. This compensation must be applied simultaneously to both the voltage and current signals to avoid any amplitude or phase errors. In this work, the filtering operation is performed using MATLAB's `filtfilt` function, resulting in zero-phase filtering and therefore avoiding phase distortion. Although such non-causal filtering cannot be directly implemented in real-time embedded systems, it allows the influence of drift compensation on impedance estimation to be evaluated independently from implementation-related constraints.

Table 1: Selected cut-off frequency.

Frequency range (Hz)	F_c (Hz)
10 to 0.1	0.1
100 to 10	9
1000 to 100	90

Each segment within every frequency range is therefore corrected using the filter and by subtracting the filtered signal from the unfiltered one, in order to remove drift and offset. The algorithm was implemented and configured in MATLAB, first to validate its operation, and then to prepare for its application to more practical cases.

4 Experimental Impedance Characterization and Model Development

To investigate the impedance behavior under dynamic operating conditions and to validate the signal processing algorithm, an experimental fuel cell model was developed. The purpose of this modeling approach is to obtain a reference model assumed to be fault-free, which can then be used to detect potential faults. It can also be used to simulate a faulty stack. In addition, the model captures the dynamic behavior of the fuel cell, making it possible to evaluate the proposed signal processing method. The objective of the model is to accurately reproduce the real impedance behavior under various operating conditions, particularly as a function of the current. To this end, electrochemical impedance spectroscopy measurements were performed under steady-state conditions on a test bench.

4.1 PEMFC test bench

To develop current-dependent impedance models of PEMFCs, experiments were carried out using a test bench developed at FCLAB (Belfort, France). These experiments are part of the "Decentralized Energy Production" project, led by EFFICACITY, the French R&D institute for urban energy transition. The monitoring and control parameters of the test bench are managed using National Instruments hardware, operated through a LabVIEW interface. More details can be found in the publications [5, 30]. The characteristics and nominal operating parameters of the fuel cell are shown in Figure 4. Air is supplied to the cathode, while a fuel mixture (75% H_2 and 25% CO_2) is supplied to the anode. The mixed fuel is set to this ratio to simulate reformate gas, since the PEMFC is designed to operate with a gas reforming system.

a)

Parameter	Value
Number of cells	12
Electrode active surface	196 cm^2
Gas distributor plates	Graphite
Fuel used during testing	75% H2 + 25% CO_2
Coolant flow: deionized water	3 l/min
Anode stoichiometry (H_2)	1.3
Cathode stoichiometry (air)	2
Anode inlet pressure	111 kPa
Air inlet pressure	106 kPa
Max. anode - cathode pressure gap	20 kPa
Temperature at cooling circuit outlet	70°C
Anode relative humidity (80°C)	50%
Cathode relative humidity (80°C)	50%
Load current	80A
Current density	0.4 $A.cm^{-2}$

b)

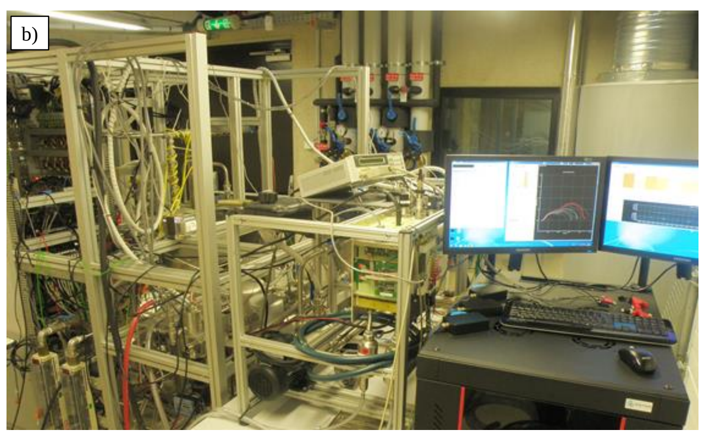

Figure 4: a) System operating parameters b) Experimental test bench designed for reference EIS.

On this bench, a spectrometer is used to perform EIS measurements according to the established operating conditions.

4.2 EIS under different conditions

Several tests were carried out on this stack, including EIS measurements performed at various operating points. These measurements were essential for developing the system's current-dependent impedance model.

For these tests, a current range was defined to cover a wide set of operating points for the stack: 20, 40, 60, 80, 100, and 120 A. Each reference EIS measurement was conducted under optimal (nominal operating), steady, and stable conditions. To obtain a model that depends solely on current, all other parameters were kept as constant as possible for each EIS. At each operating point, sufficient time was allowed for the fuel cell system to reach steady-state conditions before performing the EIS measurement. The impedance spectra were acquired using a dedicated impedance spectrometer connected to the fuel cell test bench. The stack temperature and reactant supply conditions were regulated by the fuel cell control system, ensuring comparable operating conditions between measurements. Figure 5 below shows that up to 50 A, gas flow rates were kept constant, while beyond that point, stoichiometry was controlled.

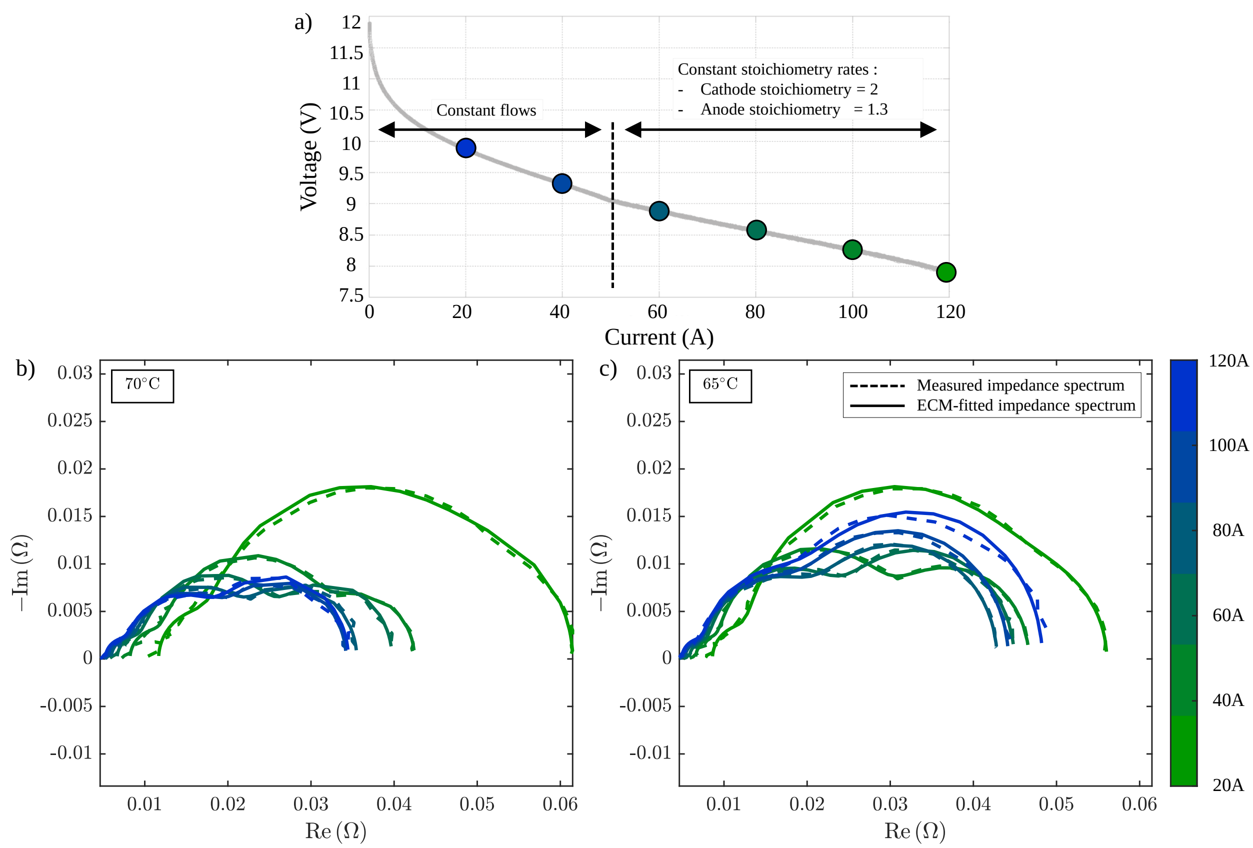

Figure 5: a) EIS operating points shown on the polarization curve, b) Reference EIS as a function of current at 70 °C, c) Reference EIS as a function of current at 65 °C.

By injecting current signals over a wide frequency range (from 0.1 Hz to 10.000 Hz), the corresponding impedance spectra were obtained. In addition, two temperatures were tested to evaluate their influence on impedance at different current levels. Although higher temperatures generally reduce charge transfer resistance through improved electrochemical kinetics, the overall impedance response results from the combined influence of several phenomena, including membrane hydration and mass transport effects.

The spectra shown in Figure 5 clearly highlight the significant influence of current on the stack's impedance. Although temperature, stoichiometry, and humidity also influence the impedance response, these parameters were intentionally regulated during the reference measurements in order to isolate the effect of current and build a current-dependent impedance model.

The objective of this study is to carry out a diagnostic analysis by monitoring potential faults that may occur during vehicle operation. Such faults can induce variations in operating parameters, including temperature, stoichiometry, and relative humidity, which in turn affect the fuel cell impedance [22]. To investigate the sensitivity of the proposed method to these impedance variations, EIS measurements were carried out under controlled variations of temperature, stoichiometry, and relative humidity (Table 2). The table reports, for each parameter, the reference value as well as the value tested under excessive (High) or deficient (Low) conditions. All EIS measurements were performed at the nominal operating current of 80 A.

Table 2: Overview of the operating conditions used to emulate fuel cell faults. For FRH conditions, the relative humidity was varied simultaneously at the anode and cathode sides.

Parameter	Reference	FSC	FT	FRH
Cathode stoichiometry	2.0	H: 2.6 / L: 1.6	2.0	2.0
Anode stoichiometry	1.3	1.5	1.3	1.3
Temperature (°C)	70	70	H: 72 / L: 62	70
Anode RH (%)	50	50	50	H: 54 / L: 46
Cathode RH (%)	50	50	50	H: 54 / L: 46

Thus, by examining the different spectra for various faults (Figure 6), whether it involves an increase or decrease in temperature (FT), stoichiometry (FSC), or relative humidity (FRH), it can be observed that the diffusive part is generally the most affected. This highlights the importance of injecting harmonics at low frequencies to obtain the maximum amount of information about the state of the fuel cell.

Now that the impedance of the fuel cell under optimal operating conditions and in the presence of faults is known, it becomes possible to build current-dependent impedance models based on the parameters of the equivalent electrical models.

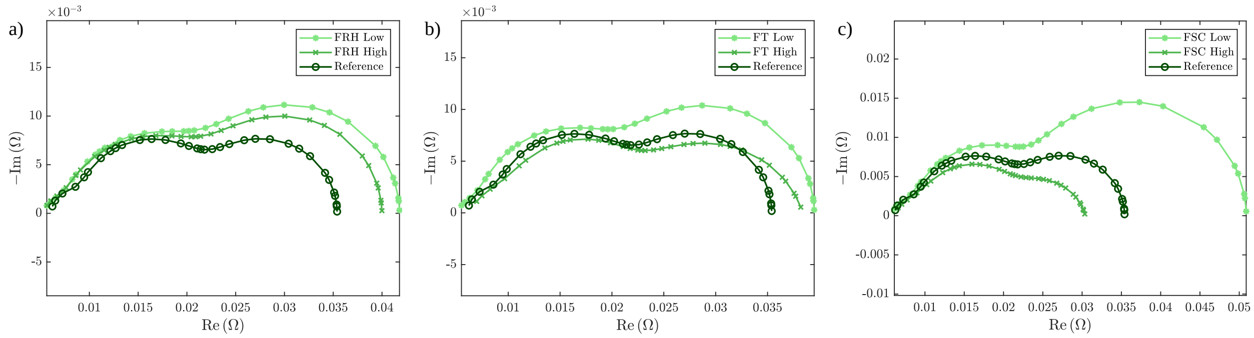

Figure 6: Reference EIS measurements recorded under various fault conditions at 70 °C and 80 A: a) relative humidity variation, b) temperature variation, c) stoichiometry variation.

4.3 Construction of the Current-dependent Impedance Model

This model serves two main purposes. First, it provides an accurate representation of the fuel cell voltage response under healthy operating conditions. Second, it enables the estimation of the ECM parameters as a function of the operating current.

The experimental fuel cell model was developed from the EIS measurements presented in Section 4.2 and implemented using the ECM shown in Figure 1. As previously discussed, this structure provides a good compromise between modeling accuracy and implementation complexity. Although CPE-based ECMs are commonly used, the selected 3RC structure was preferred because of its suitability for simulation purposes and its satisfactory fitting accuracy.

To determine the parameter values of the ECM for each current level, an optimization algorithm based on MATLAB's `fmincon` function was employed [31]. The lower bounds, initial values, and upper bounds of the optimization parameters were selected according to the work of Y. Ao et al. [5], who relied on the same experimental dataset.

Consequently, the ECM parameters were identified for each operating current, as reported in Table 3. To assess the quality of the fitting procedure, the Root Mean Square Error (RMSE) was calculated and the reconstructed impedance spectra were compared with the experimental measurements. As illustrated in Figure 5.b, the proposed ECM accurately reproduces the measured impedance spectra over the investigated operating range, with RMSE values below 0.03 for all operating points.

The ECM parameters can be associated with dominant electrochemical phenomena, as illustrated in Figure 1. However, since they are identified through a global fitting of the impedance spectrum, their values may also be influenced by interactions between several processes. Consequently, variations of the identified parameters should be interpreted as indicators of changes in the dominant electrochemical phenomena rather than as direct mea-

Table 3: Variation of ECM parameters as a function of current at 70 °C.

Parameters	20 A	40 A	60 A	80 A	100 A	120 A
R_m (Ω)	0.012	0.0085	0.0069	0.0061	0.0058	0.0055
R_a (Ω)	0.0061	0.004	0.0032	0.0029	0.0028	0.0030
C_a (F)	0.1005	0.1040	0.1251	0.1114	0.1302	0.1668
R_c (Ω)	0.0293	0.0198	0.0158	0.0130	0.0113	0.0105
C_c (F)	0.3399	0.3617	0.3955	0.4322	0.4709	0.5620
R_d (Ω)	0.0138	0.0103	0.0138	0.0134	0.0145	0.0155
C_d (F)	3.4497	9.8070	8.3390	6.0490	4.9495	4.9505
$RMSE$ (Ω)	0.0219	0.0136	0.0125	0.0113	0.0112	0.0114

surements of isolated physical quantities.

The value of each ECM parameter is therefore known at several operating points. In order to estimate parameter values between the experimentally tested currents, polynomial functions were used to interpolate the identified parameters.

To achieve a reasonable trade-off between accuracy and model simplicity, polynomial functions were employed as local approximations valid only within the considered operating range. Different polynomial orders were evaluated for each ECM parameter. Table 4 summarizes the approximation errors obtained for polynomial orders ranging from 2 to 4. Second-order polynomials were retained whenever they provided a satisfactory representation of the parameter evolution, whereas higher-order polynomials were used when necessary to capture more complex trends. Significant reductions in RMSE were observed for several parameters when increasing the polynomial order, particularly for the diffusion-related parameters. Consequently, polynomial orders ranging from 2 to 5 were selected depending on the considered parameter, providing a compromise between fitting accuracy, model simplicity, and smooth parameter evolution within the investigated operating range. The final polynomial order for each parameter was selected based on the corresponding RMSE reduction while avoiding unnecessarily complex approximations.

Table 4: RMSE obtained for different polynomial orders.

Parameter	Order 2	Order 3	Order 4
R_m	3.21×10^{-4}	5.30×10^{-5}	2.57×10^{-5}
R_a	1.93×10^{-4}	6.95×10^{-5}	2.57×10^{-6}
C_a	8.57×10^{-3}	5.95×10^{-3}	5.19×10^{-3}
R_c	7.84×10^{-4}	3.35×10^{-4}	1.11×10^{-4}
C_c	7.69×10^{-3}	4.72×10^{-3}	1.11×10^{-3}
R_d	1.10×10^{-3}	9.35×10^{-4}	5.99×10^{-4}
C_d	1.64	5.52×10^{-1}	7.43×10^{-2}

Figure 7 presents the evolution of the ECM parameters as a function of current together with the corresponding polynomial approximations.

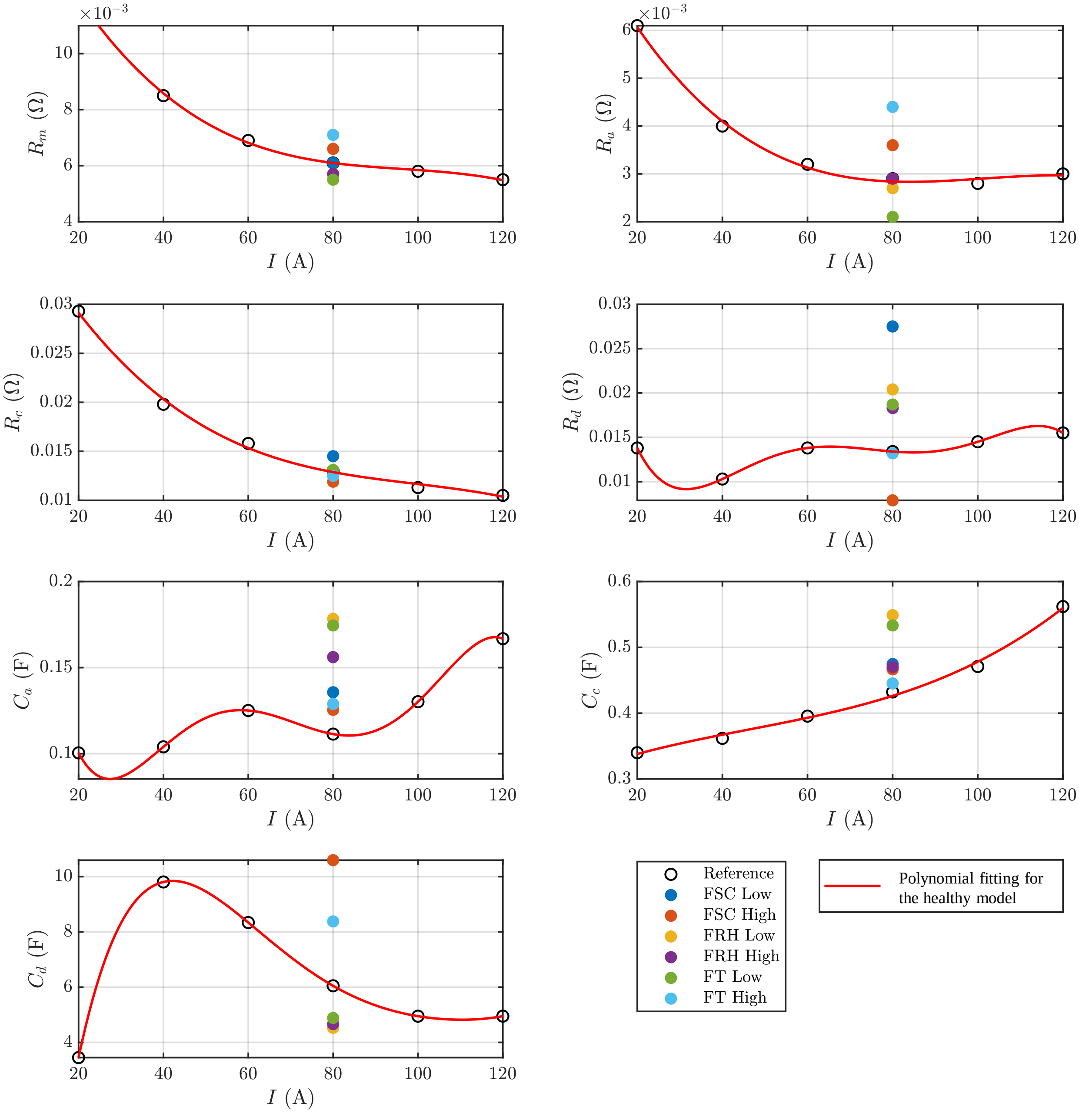

Figure 7: Current dependence of the ECM parameters identified from experimental EIS measurements. Open-circle markers correspond to healthy operating conditions, while the red curves represent the polynomial approximations used in the current-dependent model. Colored markers indicate the parameter values identified experimentally at 80 A under different fault conditions: stoichiometry fault (FSC), relative humidity fault (FRH), and temperature fault (FT).

Using the equivalent circuit model and Ohm's law, the transfer function of the fuel cell can then be expressed in the Laplace domain:

$$Z_{\text{model}} = \left\{ R_m + \frac{R_a}{1 + R_a C_a (j\omega)} + \frac{R_c}{1 + R_c C_c (j\omega)} + \frac{R_d}{1 + R_d C_d (j\omega)} \right\} \tag{2}$$

$$V_{FC}(s) = \left(R_m + \frac{R_a}{1 + R_a C_a s} + \frac{R_c}{1 + R_c C_c s} + \frac{R_d}{1 + R_d C_d s} \right) I_{FC}(s) \tag{3}$$

By combining the current-dependent parameter estimation with the ECM transfer function, a fuel cell model capable of reproducing the response of a healthy fuel cell under dynamic current profiles is obtained.

4.4 Fault Modeling

The previous section focused on the identification of a healthy current-dependent fuel cell model. To evaluate the fault detection capabilities of the proposed methodology, additional EIS measurements were performed under different fault scenarios corresponding to controlled variations of stoichiometry, temperature, and relative humidity.

Unlike the healthy dataset, which was available at several current levels, fault measurements were only available at the nominal operating point of 80 A. Consequently, current-dependent fault models could not be identified experimentally. Instead, ECM parameters were identified for each fault condition at this operating point.

Following the same identification procedure as for the healthy model, the ECM parameters associated with each fault scenario were estimated. The resulting parameter values are reported in Table 5.

Table 5: Variation of the ECM parameters under different fault conditions at 80 A.

Parameters	FSCL	FSCH	FRHL	FRHH	FTL	FTH	Reference
R_m (Ω)	0.0061	0.0066	0.0057	0.0057	0.0055	0.0071	0.0061
R_a (Ω)	0.0029	0.0036	0.0027	0.0029	0.0021	0.0044	0.0029
C_a (F)	0.1357	0.1255	0.1783	0.1561	0.1745	0.1289	0.1114
R_c (Ω)	0.0145	0.0119	0.0130	0.0130	0.0131	0.0125	0.0130
C_c (F)	0.4747	0.4666	0.5489	0.4701	0.5333	0.4452	0.4322
R_d (Ω)	0.0275	0.0079	0.0204	0.0183	0.0187	0.0132	0.0134
C_d (F)	4.5601	10.5968	4.5280	4.6626	4.8849	8.3800	6.0490
$RMSE$ (Ω)	0.0173	0.0089	0.0144	0.0135	0.0136	0.0110	0.0141

The largest parameter deviations are observed for R_d and C_d, indicating that the considered fault conditions primarily affect the low-frequency region of the impedance spectrum

(Figure 7). This observation is consistent with the impedance variations previously identified under temperature, stoichiometry, and relative humidity variations.

Since fault EIS measurements were only available at 80 A, only the ECM parameters identified at this operating point were modified to emulate the considered fault conditions. The remaining current-dependent parameter variations were retained from the healthy model. This approach makes it possible to introduce experimentally observed impedance deviations into the simulation framework while preserving the current-dependent behavior identified under healthy operating conditions.

These parameter sets represent characteristic impedance deviations associated with the considered fault scenarios and are subsequently used within the simulation framework.

5 Simulation Framework

5.1 Fuel Cell Simulation Model

The healthy current-dependent model and the fault parameter sets are combined within a common simulation environment.

The fuel cell model is built from the ECM transfer functions (Eq. 2 and Eq. 3) together with the current-dependent parameter estimation obtained from the polynomial relationships. The fuel cell current is used as the model input, while the cell voltage is obtained as the output.

Under healthy operating conditions, the polynomial models identified from the experimental EIS measurements are used to estimate the ECM parameters over the full operating range. These parameters are then introduced into the transfer function to reproduce the fuel cell response under dynamic current profiles.

To simulate a fault, the healthy parameter value identified at 80 A is replaced by the corresponding faulty parameter value identified experimentally at the same operating point, while the remaining operating points retain their healthy values. The resulting dataset is then used to generate a new set of polynomial relationships representative of the considered fault scenario. In this way, experimentally observed fault-induced impedance deviations can be incorporated into the current-dependent model.

Depending on the selected scenario, the resulting model reproduces the impedance variations associated with stoichiometry, temperature, or relative humidity faults. This approach makes it possible to simulate both healthy and faulty operating conditions under dynamic current profiles. The resulting voltage and current signals are then used to evaluate the proposed impedance estimation and fault detection methodology.

5.2 Power Converter Model

Modeling the power converter makes it possible to test the dynamic EIS method under realistic conditions. By coupling a power converter model with the experimental fuel cell model, the complete methodology can be validated and brought closer to actual onboard systems.

At this stage, in order to better represent onboard operating conditions, the signal injection must be carried out through the power converter. A converter model was therefore developed, based on a boost converter architecture that steps up the fuel cell voltage to the reference DC bus voltage. The topology of the converter is shown in Figure 8.

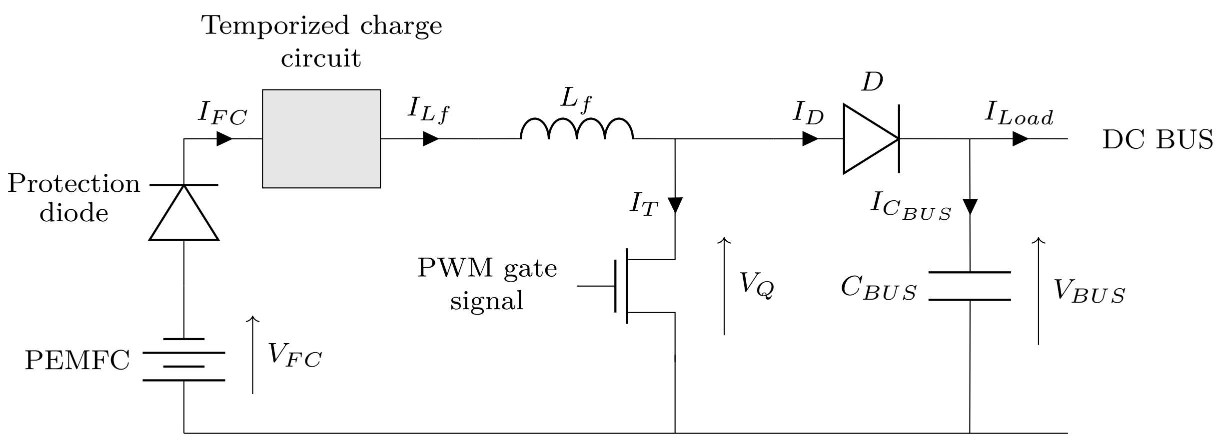

Figure 8: Modeled electrical circuit of the boost converter including the PEMFC, protection diode and temporized charge circuit.

This converter was modeled in Simulink and coupled with the fuel cell model. To inject the current stimulus, the PWM is modulated accordingly. The multi-sine signal is added to the reference current requested by the DC bus, which allows the signal to be automatically modulated.

The converter is controlled using a current regulation loop and a PWM switching strategy. The role of the converter is not to provide the excitation frequencies required for impedance estimation, but to inject the multi-sine excitation signal into the fuel cell current while maintaining realistic operating conditions representative of onboard applications.

By superimposing the multi-sine signal onto the current reference, several frequencies can be injected simultaneously through the converter. This significantly reduces the duration of the EIS measurement while preserving the ability to estimate impedance over a wide frequency range.

Thus, the proposed signal processing method can be evaluated on the current-dependent impedance model by applying current stimuli via the modeled converter to detect possible faults.

6 Validation of the Dynamic EIS Methodology

After developing the current-dependent fuel cell model and the associated power converter model, the next step is to evaluate the proposed dynamic EIS methodology within the developed simulation framework. Two case studies are considered: a first test under controlled operating conditions and a second test under dynamic current conditions. These simulations are used to assess the ability of the developed signal processing algorithm to estimate impedance spectra under non-stationary operating conditions and to compare the obtained results with the reference experimental EIS measurements used for model identification.

6.1 Validation of the Dynamic EIS Method under Static Conditions

To evaluate the proposed dynamic EIS methodology, impedance data were generated using the current-dependent fuel cell model under controlled operating conditions. Current stimuli covering the entire frequency range were injected through the power converter.

As highlighted in several studies [8], injection via the converter can introduce noise and thus affect the results. However, using appropriate analog anti-aliasing filters and suitable decimation techniques helps minimize these effects.

Table 6: Signal processing algorithm parameters.

Sampling frequency before decimation	*4800 Hz*		
Windowing	*Hamming*		
Averaging	*Depends on the stimulus injection time for each operating point range*		
Number of points per segment	*128*		
Frequency ranges	*HF*	*MF*	*LF*
Decimation	*1*	*25*	*250*
Duration of the segments	*27 ms*	*667 ms*	*6.30 sec*
Overlap	*50 %*	*80 %*	*90 %*
Cutoff frequency of the anti-aliasing filter	*960 Hz*	*96 Hz*	*9.6 Hz*
Cutoff frequency of the low-pass filter	*90 Hz*	*9 Hz*	*0.1 Hz*

The goal here is to demonstrate the feasibility of the method using the developed algorithm. This algorithm does not require prior knowledge of the injected frequencies or synchronization between signal processing and the injection itself. The algorithm was configured according to the parameter values shown in Table 6, allowing the analysis of three distinct frequency ranges, as previously presented.

An operating point of 80 A was selected, and ten frequencies were injected using a multi-sine signal (Figure 9.a). The figure below shows the comparison between the reference impedance and the impedance estimated from the model and the algorithm.

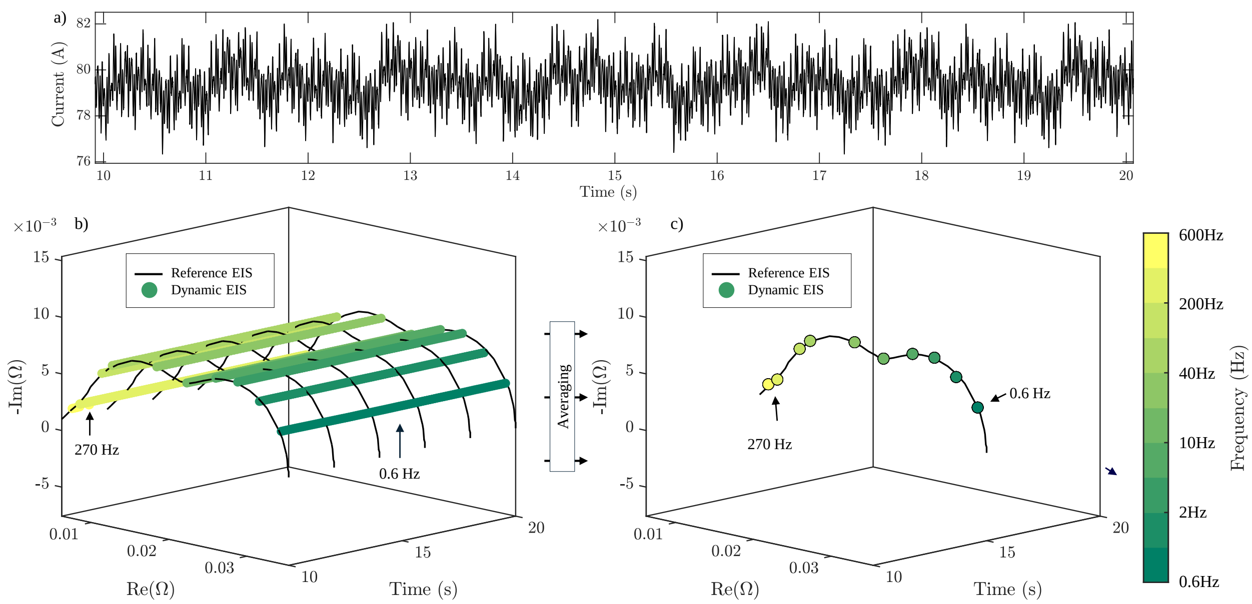

Figure 9: a) Current signal containing the injected multi-sine excitation around the 80 A operating point, b) Impedance spectra identified from all analysis segments over the 10 s measurement window, c) Averaged impedance spectrum resulting from these individual estimates and comparison with the reference EIS.

By examining the spectrum in Figure 9, it can be seen that the reference spectrum and the measured impedance at the various injected frequencies match perfectly. Due to the segmentation method described in previous sections, an averaging is performed over a 10-second period for each detected frequency.

The agreement between the dynamic EIS estimates and the reference EIS spectra was quantified by interpolating the reference impedance at the estimated measurement frequencies. The RMSE of the complex impedance was $1.37\times10^{-4}\,\Omega$, and the mean relative deviation of $|Z|$ was 0.56% (maximum: 2.04%), confirming the excellent match shown in Figure 9.

This validation demonstrates that it is possible to determine the impedance spectrum without prior knowledge of the injected frequencies, within a total duration of 10 seconds. In a second step, it is useful to verify the performance of the entire method under dynamic conditions.

6.2 Validation of the Dynamic EIS Method under Dynamic Conditions

In this second case study, the same frequencies were injected while the fuel cell model was subjected to a dynamic current profile. To achieve this, a current ramp ranging from 10 A to 120 A was applied. EIS measurements were performed every 5 seconds, each over a duration of 10 seconds (Figure 10.a). The acquired voltage and current signals were then processed using the developed algorithm, and the results are presented below.

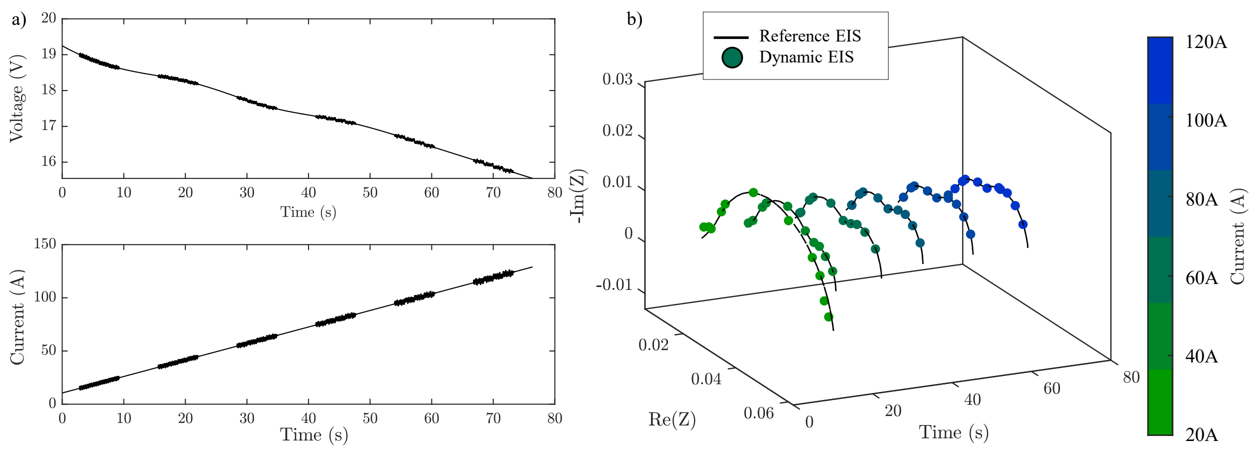

Figure 10: a) Measured dynamic current and voltage profiles, b) Comparison between the impedance estimated under dynamic operating conditions (Dynamic EIS) and the ECM reconstructed from the reference experimental EIS measurements obtained under steady-state conditions.

The spectra in Figure 10.b show that the impedance estimated under dynamic operating conditions remains consistent with the ECM representations identified from the reference experimental EIS measurements. This result demonstrates that the proposed dynamic EIS methodology is able to recover impedance characteristics obtained experimentally under steady-state conditions while the fuel cell operates under a dynamic current profile.

These results support the feasibility of the proposed methodology within the developed simulation framework and provide a basis for investigating fault detection under representative driving-cycle conditions. Since the objective of this work is the proof-of-concept validation of the methodology, the assessment is primarily based on the agreement between the reconstructed impedance spectra and the experimental reference spectra used for model identification.

7 Fault Detection on a Representative Driving Cycle

The objective of this study is to investigate fault detection under dynamic operating conditions. To achieve this, a driving profile representative of real vehicle operation (Lyon–Milan cycle) was applied to the developed simulation model.

7.1 Driving Cycle and Stimulus Injection Protocol

The driving cycle data used in this study were collected during a real trip between Lyon (France) and Milan (Italy), carried out by a 44-ton hydrogen-powered truck. The DC bus power was measured from the current and voltage, with a sampling frequency of 1 Hz over a duration of 7 hours (Figure 11).

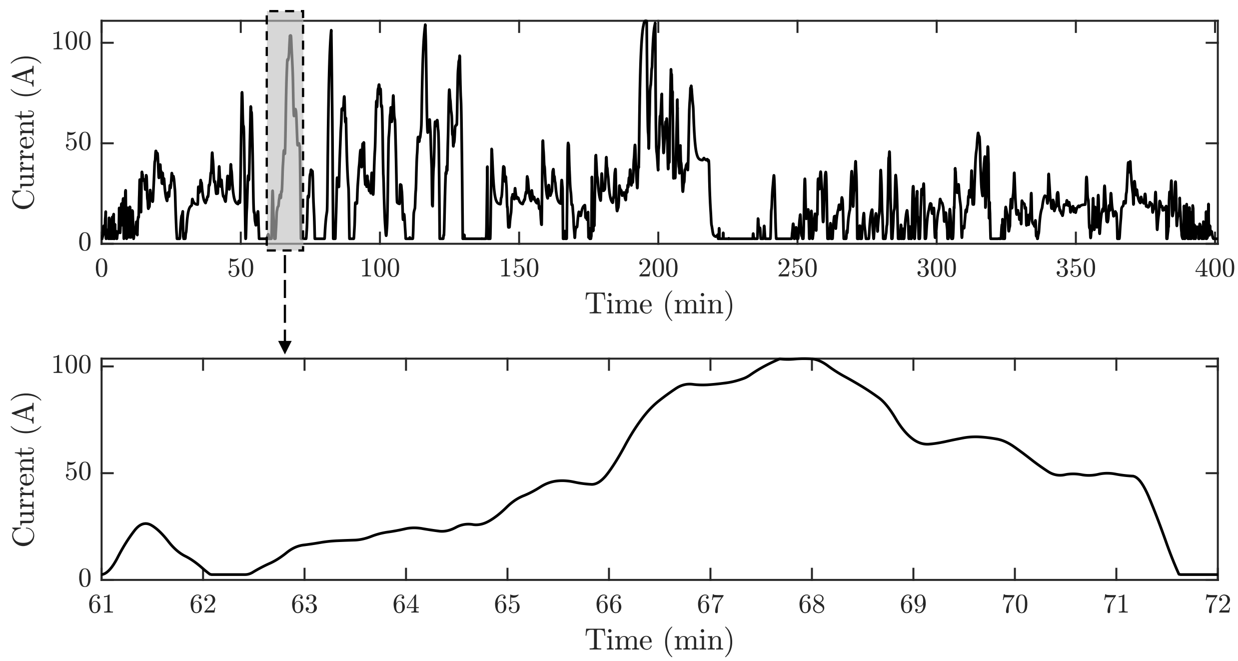

Figure 11: Lyon-Milan driving cycle used in the study.

Based on approaches widely reported in the literature [32], an energy management strategy was implemented to estimate the current drawn from the fuel cell, focusing on its slow dynamics. Specifically, a low-pass filtering approach combined with a minimum power saturation was used to prevent the fuel cell from stopping.

Thanks to this energy management strategy, the contribution of the fuel cell is oriented toward low-frequency components of the load, while higher-frequency variations are handled by the battery. This approach allows a realistic estimation of the fuel cell current while ensuring smooth operation and avoiding frequent power fluctuations, consistent with the methods reported in the literature.

In the following section of the study, 11 minutes of the driving cycle are analyzed, with a sampling rate of 4.8 kHz. A specific strategy was implemented for performing EIS. For validation purposes, the signal injection is triggered when the current is within ± 5 A of the operating points for which reference EIS measurements are available. This criterion is introduced solely to enable comparison with the experimental reference spectra and does not constitute a requirement of the proposed dynamic EIS methodology. In principle, the methodology can be applied at any operating current, since the current-dependent impedance model provides parameter estimates over the entire investigated operating range.

These operating points correspond to those studied in the laboratory, allowing a comparison with the reference EIS measurements. A real-time current measurement is used to trigger the injection of the sinusoidal signal through the converter as soon as the current enters a valid range.

In this way, several dozen frequencies are injected in the form of a multi-sine signal, allowing the tracking of impedance spectrum variations over a short period of time under dynamic current conditions.

Two case studies were tested:

- The first using a fault-free model,
- The second by introducing a cathode stoichiometry fault (FSC Low), randomly injected during the 11-minute simulation.

7.2 Impedance Monitoring

The 11-minute segment of the Lyon-Milan driving cycle described above was replayed on the fuel cell model, with the EIS harmonics injected through the power converter. The voltage and current signals were then acquired at a sampling frequency of 4.8 kHz so they could be processed by the developed signal-processing algorithm.

In both the fault-free and faulty simulations, the same algorithm parameters as in the previous sections were used. With the method now implemented, the two case studies can be analyzed.

In this study, the objective is to assess whether impedance variations caused by a fault can still be detected under dynamic operating conditions. First, the embedded impedance measurements are compared with reference EIS data used to establish the healthy model. Then, to detect a fault, a 10% threshold is applied to the resistive and capacitive parameters of the healthy fuel cell ECM. This criterion makes it possible to determine whether the estimated ECM parameters remain within an acceptable range. Any deviation beyond this interval indicates the presence of a potential fault. The 10% threshold was selected as a simple engineering criterion for this proof-of-concept study. This value was chosen to remain significantly larger than the impedance reconstruction errors observed during the validation stage, thereby reducing the likelihood of detecting variations caused solely by estimation uncertainties. A dedicated analysis of threshold optimization, false positives, and false negatives is beyond the scope of the present work and will be investigated in future studies.

7.2.1 Fault-free case

The black curves correspond to the reference spectrum for each operating point studied. The points ranging from dark blue to navy represent the impedances measured through the current stimuli injected via the power converter (Figure 12.a).

Figure 12.b shows the tracking of impedance spectra at the times when the sinusoidal signals were injected. Specifically, it illustrates how the impedance evolves with the current.

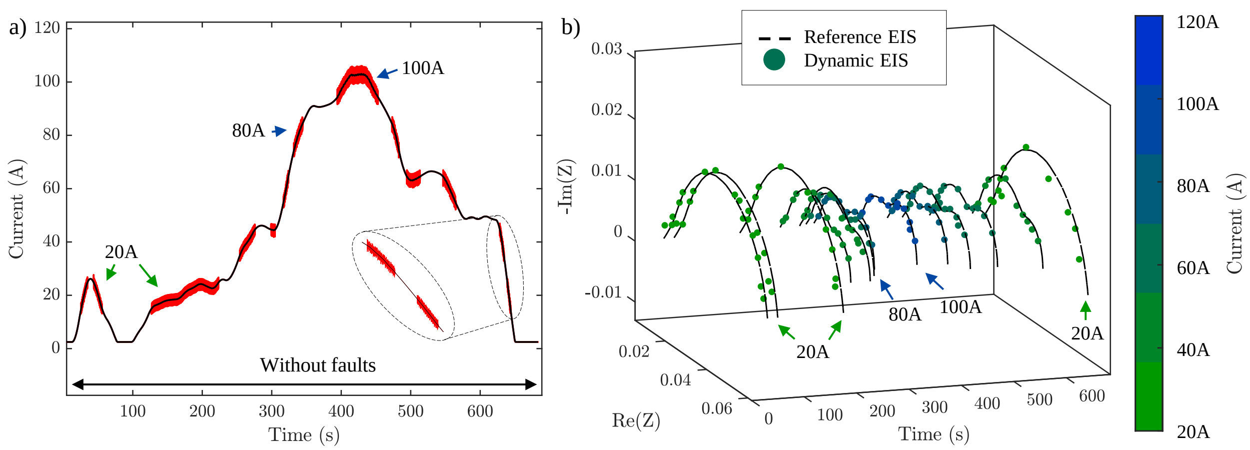

Figure 12: a) Lyon-Milan driving cycle with current stimuli injection, b) Dynamic EIS measurements (green markers) compared with the ECM-reconstructed spectra obtained from the reference experimental EIS measurements (black dashed lines) for different operating currents.

By examining these spectra, a strong agreement can be observed between the reference EIS measurements and those obtained during active operation. This demonstrates the feasibility that, even under dynamic conditions, it is possible to recover the impedance without having to impose a steady-state operating regime on the power source.

In this study, the model relies solely on the current, which made it possible to confirm that the spectra can be accurately obtained under dynamic operating conditions. However, for models that include additional parameters, such as temperature or other variables, the duration of the EIS measurement becomes a critical factor. This is precisely where the main advantage of the developed method lies. Indeed, each EIS measurement is performed over a very short period, typically between 10 and 15 seconds. This is an important point, as it allows multiple EIS measurements to be taken in a short time.

7.2.2 Faulty case

Now that it is possible to track impedance under dynamic current conditions, the next objective is to introduce a fault into the model in order to detect it through the impedance spectra. As shown in the previous sections, reference EIS measurements were carried out at 80 A for different fault levels. The corresponding values of the equivalent electrical model parameters were then integrated into the current-dependent impedance model.

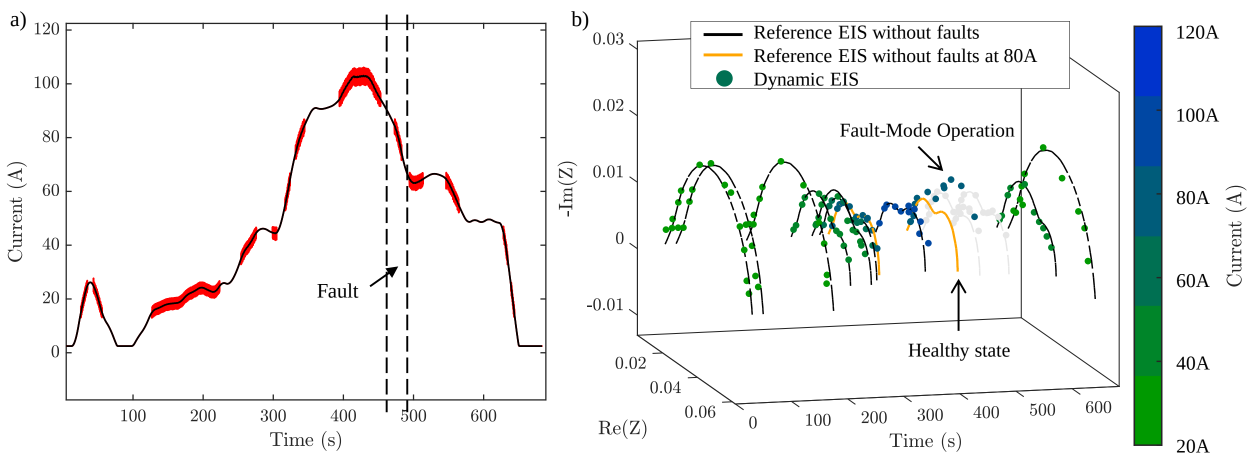

Figure 13: a) Lyon-Milan driving cycle with fault injection, b) Evolution of the estimated impedance spectra before and after fault occurrence.

By applying the same Lyon-Milan driving cycle and introducing a fault between 440 and 480 seconds, the goal is to identify this fault through impedance spectrum analysis. Figure 13 illustrates the different stages of this detection process:

- Plot a): shows the moments when the current stimuli are injected, as well as the exact moment when the fault is introduced;
- Plot b): presents the impedance spectra obtained under dynamic conditions, with a visible fault at 80 A. The fault is identified by the deviation between the reference and the measured spectra. The curves are shown in grey to enhance the visibility of the detected fault;

A fault is considered to be detected when deviations exceeding 10% are observed in multiple ECM parameters with respect to the healthy current-dependent model.

The proposed methodology successfully detects the presence of the introduced fault through the resulting impedance variations.

This study has demonstrated that it is possible to detect faults under dynamic current conditions without interrupting the power source, within a short time, and without requiring system synchronization.

8 Conclusion

This paper presents a current-dependent fuel cell impedance model for both healthy and faulty operating conditions and investigates the feasibility of dynamic EIS for fault detection under dynamic operating conditions. Based on this framework, dynamic EIS was investigated under realistic operating conditions. To achieve this objective, several steps were carried out:

- EIS measurements were first performed under different steady-state operating conditions as a function of current, in order to identify its influence on the impedance response.

- Polynomial relationships were then established to estimate the ECM parameters as a function of current. Combined with the ECM transfer function, this approach made it possible to simulate dynamic current profiles and reproduce the fuel cell behavior under both steady-state and transient operating conditions.

- In order to compute impedance under dynamic conditions, a dedicated signal processing algorithm was developed to compensate for drift and extract impedance spectra over very short time windows, without interrupting the power delivery. This method demonstrated the feasibility of embedded impedance measurements, as confirmed by several validation tests.

- Using this simulation framework, impedance spectra were reconstructed under the Lyon-Milan driving cycle and successfully applied to fault detection.

The results demonstrate the feasibility of detecting faults under dynamic operating conditions using the proposed dynamic EIS methodology. Future work will focus on extending this framework by incorporating additional operating parameters of the fuel cell stack (temperature, relative humidity), in order to cover a wider range of fault modes and improve fault discrimination and diagnosis.

Acknowledgments

This work has been supported by the EIPHI Graduate school (contract "ANR-17-EURE-0002" and the Region of Bourgogne Franche-Comté).

The HYSySPEM project was funded by the “France 2030” government investment plan managed by the French National Research Agency, under the reference ANR-22-PEHY-0018.

This work was supported by a grant from the French State, managed by the National Research Agency under the Investments for the Future program, reference ANR-21-ESRE-0033.

Declaration of Competing Interest

The authors declare that they have no known competing financial interests or personal relationships that could have appeared to influence the work reported in this paper.

References

[1] Forum International des Transports. *Perspectives des transports FIT 2023*. en. Perspectives des transports FIT. OECD, Apr. 2024. ISBN: 978-92-821-1630-2 978-92-821-1507-7 978-92-821-1823-8. DOI: 10.1787/32bbcca5-fr.

[2] Fangjie Liu, Muhammad Shafique, and Xiaowei Luo. “Dynamic lifecycle emissions of electric and hydrogen fuel cell vehicles in a multi-regional perspective”. en. In: *Environmental Impact Assessment Review* 111 (Jan. 2025), p. 107695. ISSN: 01959255. DOI: 10.1016/j.eiar.2024.107695.

[3] R. Petrone et al. “A review on model-based diagnosis methodologies for PEMFCs”. en. In: *International Journal of Hydrogen Energy* 38.17 (June 2013), pp. 7077–7091. ISSN: 03603199. DOI: 10.1016/j.ijhydene.2013.03.106.

[4] R. Onanena et al. “Fuel cells static and dynamic characterizations as tools for the estimation of their ageing time”. en. In: *International Journal of Hydrogen Energy* 36.2 (Jan. 2011), pp. 1730–1739. ISSN: 03603199. DOI: 10.1016/j.ijhydene.2010.10.064.

[5] Yunjin Ao, Salah Laghrouche, and Daniel Depernet. “Diagnosis of proton exchange membrane fuel cell system based on adaptive neural fuzzy inference system and electrochemical impedance spectroscopy”. en. In: *Energy Conversion and Management* 256 (Mar. 2022), p. 115391. ISSN: 01968904. DOI: 10.1016/j.enconman.2022.115391.

[6] Slimane Laribi et al. "Analysis and diagnosis of PEM fuel cell failure modes (flooding & drying) across the physical parameters of electrochemical impedance model: Using neural networks method". en. In: *Sustainable Energy Technologies and Assessments* 34 (Aug. 2019), pp. 35–42. ISSN: 22131388. DOI: 10.1016/j.seta.2019.04.004.

[7] Christian Jeppesen et al. "An EIS alternative for impedance measurement of a high temperature PEM fuel cell stack based on current pulse injection". en. In: *International Journal of Hydrogen Energy* 42.24 (June 2017), pp. 15851–15860. ISSN: 03603199. DOI: 10.1016/j.ijhydene.2017.05.066.

[8] Daniel Depernet et al. "Integration of electrochemical impedance spectroscopy functionality in proton exchange membrane fuel cell power converter". en. In: *International Journal of Hydrogen Energy* 41.11 (Mar. 2016), pp. 5378–5388. ISSN: 03603199. DOI: 10.1016/j.ijhydene.2016.02.010.

[9] J. Sihvo and D-I. Stroe. "Real-time impedance monitoring of Li-ion batteries under dynamic operating conditions using the discrete Fourier transform eigenvector approach". en. In: *Cell Reports Physical Science* (Mar. 2025), p. 102512. ISSN: 26663864. DOI: 10.1016/j.xcrp.2025.102512.

[10] Yanlin Xiao et al. "Rapid detection of dynamic electrochemical impedance spectroscopy of batteries based on sampling function excitation". en. In: *Journal of Power Sources* 641 (June 2025), p. 236823. ISSN: 03787753. DOI: 10.1016/j.jpowsour.2025.236823.

[11] Bernhard Liebhart, Lidiya Komsiyska, and Christian Endisch. "Passive impedance spectroscopy for monitoring lithium-ion battery cells during vehicle operation". en. In: *Journal of Power Sources* 449 (Feb. 2020), p. 227297. ISSN: 03787753. DOI: 10.1016/j.jpowsour.2019.227297.

[12] Bernhard Liebhart et al. "Enhancing the Cell Impedance Estimation of a Lithium-Ion Battery System with Embedded Power Path Switches". en. In: *2021 IEEE Applied Power Electronics Conference and Exposition (APEC)*. Phoenix, AZ, USA: IEEE, June 2021, pp. 967–974. ISBN: 978-1-7281-8949-9. DOI: 10.1109/APEC42165.2021.9487173.

[13] Xilei Sun et al. "Boosted deep neural network model for forecasting the electrochemical impedance of a proton exchange membrane fuel cell under varying operating conditions". In: *Renewable Energy* 256 (Jan. 2026), p. 124099. ISSN: 0960-1481. DOI: 10.1016/j.renene.2025.124099.

[14] Nils Lohmann et al. "Electrochemical impedance spectroscopy for lithium-ion cells: Test equipment and procedures for aging and fast characterization in time and frequency

domain". en. In: *Journal of Power Sources* 273 (Jan. 2015), pp. 613–623. ISSN: 03787753. DOI: 10.1016/j.jpowsour.2014.09.132.

[15] Alexandros Ch. Lazanas and Mamas I. Prodromidis. "Electrochemical Impedance SpectroscopyA Tutorial". en. In: *ACS Measurement Science Au* 3.3 (June 2023), pp. 162–193. ISSN: 2694-250X, 2694-250X. DOI: 10.1021/acsmeasuresciau.2c00070.

[16] C. A. Schiller et al. "Validation and evaluation of electrochemical impedance spectra of systems with states that change with time". en. In: *Physical Chemistry Chemical Physics* 3.3 (2001), pp. 374–378. ISSN: 14639076, 14639084. DOI: 10.1039/b007678n.

[17] D. Hissel and M.C. Pera. "Diagnostic & health management of fuel cell systems: Issues and solutions". en. In: *Annual Reviews in Control* 42 (2016), pp. 201–211. ISSN: 13675788. DOI: 10.1016/j.arcontrol.2016.09.005.

[18] Thomas Génevé, Jérémi Régnier, and Christophe Turpin. "Fuel cell flooding diagnosis based on time-constant spectrum analysis". en. In: *International Journal of Hydrogen Energy* 41.1 (Jan. 2016), pp. 516–523. ISSN: 03603199. DOI: 10.1016/j.ijhydene.2015.10.089.

[19] Walter Zamboni et al. "An Evolutionary Computation Approach for the Online/On-Board Identification of PEM Fuel Cell Impedance Parameters with A Diagnostic Perspective". en. In: *Energies* 12.22 (Jan. 2019). Publisher: Multidisciplinary Digital Publishing Institute, p. 4374. ISSN: 1996-1073. DOI: 10.3390/en12224374.

[20] Ángel Hernández-Gómez et al. "Development of an Equivalent Electronic Circuit Model for PEMFC Voltage Based on Different Input Electrical Currents". en. In: *IEEE Access* 11 (2023), pp. 108328–108338. ISSN: 2169-3536. DOI: 10.1109/ACCESS.2023.3320936.

[21] Norbert Wagner. "Electrochemical Impedance Spectroscopy". en. In: *PEM Fuel Cell Diagnostic Tools*. Ed. by Hui Li. CRC Press, Aug. 2011, pp. 37–70. ISBN: 978-1-4398-3919-5 978-1-4398-3920-1. DOI: 10.1201/b11100-5.

[22] Hao Yuan et al. "Understanding dynamic behavior of proton exchange membrane fuel cell in the view of internal dynamics based on impedance". en. In: *Chemical Engineering Journal* 431 (Mar. 2022), p. 134035. ISSN: 13858947. DOI: 10.1016/j.cej.2021.134035.

[23] Lei Zhao et al. "Inconsistency evaluation of vehicle-oriented fuel cell stacks based on electrochemical impedance under dynamic operating conditions". en. In: *Energy* 265 (Feb. 2023), p. 126162. ISSN: 03605442. DOI: 10.1016/j.energy.2022.126162.

[24] Jianfeng Lv et al. “Diagnosis of PEM Fuel Cell System Based on Electrochemical Impedance Spectroscopy and Deep Learning Method”. en. In: *IEEE Transactions on Industrial Electronics* 71.1 (Jan. 2024), pp. 657–666. ISSN: 0278-0046, 1557-9948. DOI: 10.1109/TIE.2023.3241404.

[25] Hao Yuan et al. “Unconventional frequency response analysis of PEM fuel cell based on high-order frequency response function and total harmonic distortion”. en. In: *Applied Energy* 357 (Mar. 2024), p. 122489. ISSN: 03062619. DOI: 10.1016/j.apenergy.2023.122489.

[26] Zhe Zhang et al. “A review of power converter-based online electrochemical impedance spectroscopy for electrochemical devices in electric vehicles”. en. In: *eTransportation* 25 (Sept. 2025), p. 100453. ISSN: 25901168. DOI: 10.1016/j.etran.2025.100453.

[27] Xutao Liu et al. “Binary multi-frequency signal for accurate and rapid electrochemical impedance spectroscopy acquisition in lithium-ion batteries”. en. In: *Applied Energy* 364 (June 2024), p. 123221. ISSN: 03062619. DOI: 10.1016/j.apenergy.2024.123221.

[28] Bernhard Liebhart et al. “Improved Impedance Measurements for Electric Vehicles with Reconfigurable Battery Systems”. en. In: *2021 IEEE 12th Energy Conversion Congress & Exposition - Asia (ECCE-Asia)*. Singapore, Singapore: IEEE, May 2021, pp. 1736–1742. ISBN: 978-1-7281-6344-4. DOI: 10.1109/ECCE-Asia49820.2021.9479060.

[29] F.J Owens and M.S Murphy. “A short-time Fourier transform”. en. In: *Signal Processing* 14.1 (Jan. 1988), pp. 3–10. ISSN: 01651684. DOI: 10.1016/0165-1684(88)90040-0.

[30] D. Benouioua et al. “On the issue of the PEMFC operating fault identification: Generic analysis tool based on voltage pointwise singularity strengths”. en. In: *International Journal of Hydrogen Energy* 43.25 (June 2018), pp. 11606–11613. ISSN: 03603199. DOI: 10.1016/j.ijhydene.2017.09.177.

[31] Tummala.S.L.V. Ayyarao, Nishanth Polumahanthi, and Baseem Khan. “An accurate parameter estimation of PEM fuel cell using war strategy optimization”. en. In: *Energy* 290 (Mar. 2024), p. 130235. ISSN: 03605442. DOI: 10.1016/j.energy.2024.130235.

[32] Sara Luciani and Andrea Tonoli. “Control Strategy Assessment for Improving PEM Fuel Cell System Efficiency in Fuel Cell Hybrid Vehicles”. en. In: *Energies* 15.6 (Mar. 2022), p. 2004. ISSN: 1996-1073. DOI: 10.3390/en15062004.